


RESEARCH ARTICLE

Severe histomorphological alterations in post-mortem olfactory glomeruli in Alzheimer's disease

Gwoon Son^{1,2,3} | Harry W. M. Steinbusch^{1,3} | Carmen López-Iglesias⁴ | Cheil Moon^{1,5,6} | Ali Jahanshahi^{2,3} 

¹Department of Brain & Cognitive Sciences, Graduate School, Daegu Gyeungbuk Institute of Science and Technology, Daegu, Republic of Korea

²Department of Neurosurgery, Maastricht University Medical Center+, Maastricht, The Netherlands

³School for Mental Health and Neuroscience, Maastricht University, Maastricht, The Netherlands

⁴Microscopy CORE Lab, Maastricht Multimodal Molecular Imaging Institute, FHML, Maastricht University, Maastricht, The Netherlands

⁵Convergence Research Advanced Centre for Olfaction, Daegu Gyeungbuk Institute of Science and Technology, Daegu, Republic of Korea

⁶Korea Brain Research Institute, Daegu, Republic of Korea

Correspondence

Ali Jahanshahi, Department of Neurosurgery, Maastricht University Medical Center+, P. Debyelaan 25, Maastricht 6229 HX, The Netherlands.
Email: a.jahanshahi@maastrichtuniversity.nl

Cheil Moon, Department of Brain & Cognitive Sciences, Graduate School, DGIST, Techno-Joongangdaero 333, Dalseong-gun, Daegu 42988, Republic of Korea.
Email: cmoon@dgist.ac.kr

Funding information

This work was supported by research grant from the KBRI basic research program through Korea Brain Research Institute funded by the Ministry of Science and ICT (18-BR-04-01) and Basic Science Research Program through the National Research Foundation of Korea (NRF) funded by the Ministry of Education (2020R1A6A1A03040516). Funding was also provided from Maastricht University through the School for Mental Health and Neuroscience. The funding sources had no such involvement in study design; in the collection, analysis and interpretation of data; in the writing of the report; and in the decision to submit the article for publication

Abstract

Alzheimer's disease (AD) is the most prevalent form of dementia. Key AD symptoms include memory and cognitive decline; however, comorbid symptoms such as depression and sensory-perceptual dysfunction are often reported. Among these, a deterioration of olfactory sensation is observed in approximately 90% of AD patients. However, the precise pathophysiological basis underlying olfactory deficits because of AD remains elusive. The olfactory glomeruli in the olfactory bulb (OB) receive sensory information in the olfactory processing pathway. Maintaining the structural and functional integrity of the olfactory glomerulus is critical to olfactory signalling. Herein, we conducted an in-depth histopathological assessment to reveal detailed structural alterations in the olfactory glomeruli in AD patients. Fresh frozen post-mortem OB specimens obtained from six AD patients and seven healthy age-matched individuals were examined. We used combined immunohistochemistry and stereology to assess the gross morphology and histological alterations, such as those in the expression of A β protein, microglia, and neurotransmitters in the OB. Electron microscopy was employed to study the ultrastructural features in the glomeruli. Significant accumulation of A β , morphologic damage, altered neurotransmitter levels, and microgliosis in the olfactory glomeruli of AD patients suggests that glomerular damage could affect olfactory function. Moreover, greater neurodegeneration was observed in the ventral olfactory glomeruli of AD patients. The synaptic ultrastructure revealed distorted postsynaptic densities and a decline in presynaptic vesicles in AD specimens. These findings show that the primary

Cheil Moon and Ali Jahanshahi are contributed equally to this work.

This is an open access article under the terms of the Creative Commons Attribution-NonCommercial-NoDerivs License, which permits use and distribution in any medium, provided the original work is properly cited, the use is non-commercial and no modifications or adaptations are made.

© 2021 The Authors. *Brain Pathology* published by John Wiley & Sons Ltd on behalf of International Society of Neuropathology.

olfactory pathway is affected by the pathogenesis of AD, and may provide clues to identifying the mechanism involved in olfactory dysfunction in AD.

KEYWORDS

Alzheimer's disease, morphology, olfactory bulb, post-mortem histology, ultrastructure

1 | INTRODUCTION

Alzheimer's disease (AD) is a neurodegenerative disease that accounts for 60–80% of all dementia cases [1]. Primary AD symptoms include memory and cognitive decline, depression, and sensory-perceptual dysfunction [2, 3]. Deterioration in smelling function is a common symptom that affects approximately 90% of AD patients [4]. Since olfactory dysfunction occurs in the early stages of the disease, studying its underlying pathophysiological processes could help to understand its mechanisms and help to develop tools for early diagnosis. So far, neuropathological alterations in cortical olfactory areas have been considered as the main cause of smelling deficits in AD [5]. Nevertheless, non-cortical areas, especially the olfactory bulbs (OB), have recently gained a considerable deal of attention.

The human olfactory system comprises the primary and the secondary olfactory pathway. In the primary olfactory pathway, the olfactory sensory neurons (OSNs) in the OE encounter odorants and project their axons to the OB. Thus, the OB hosts the first synapse in the primary olfactory processing pathway [6]. OSN synapses, namely the olfactory glomeruli, are spherical neuropil structures that wire both peripheral and central neurons [7]. Olfactory glomeruli act as the site for encoding olfactory signals, and a gateway to the secondary olfactory pathway. In turn, OSNs expressing a specific odorant receptor gene project their sensory information along their axons to specific glomeruli with highly precise stereotypy, where they form synapses with mitral/tufted cells and sharpen olfactory signals via lateral inhibition [8]. Ample evidence suggests that these topographical characteristics play a crucial role in the sense of smell [9]. Therefore, maintaining the structural integrity of the olfactory glomerulus is essential for olfactory signalling [10]. In vivo studies on rodents have indicated that damaged olfactory glomeruli could contribute to olfactory dysfunction in mice [11].

The expression of β -amyloid (A β) plaques is the cardinal pathological hallmark in the brains of patients with AD. Aggregated A β proteins are positively associated with impaired synaptic transmission and neural network malfunction [12]. Animal studies have shown that amyloidosis of amyloid precursor proteins in presynaptic terminals reduces excitatory transmitter release and results in A β -induced synaptic deficits [13]. Moreover, these synaptic deficits induce postsynaptic depression by

suppressing long-term potentiation or promoting long-term depression [14]. Additionally, the accumulation of A β proteins can trigger sequential pathogenic cascades such as microglial reactivation and infiltration around damaged neurons by driving disrupting neurotransmitter release and accelerating amyloidopathy [15, 16]. In AD, the accumulation of A β proteins and abnormal neuroinflammatory processes can cause structural deficits and functional instability in the neural networks. A β protein expression has already been reported in the primary olfactory pathway of pathologically verified AD patients [17]. Gliosis has also been shown to impair cell signalling in the OB of AD patients [18]. However, it is not clear how and to what extent these aggregates play a role in the pathophysiology of olfactory impairment.

Herein, we assessed the morphological and histochemical alterations in the olfactory glomeruli of the OB obtained from clinically confirmed AD patients and age-matched controls (CTLs). We addressed whether the structural integrity of the olfactory glomeruli could be affected by A β protein expression and microgliosis in individuals with AD. To this end, we used designed-based stereology and immunohistochemical analysis as tools to assess pathological and morphological changes in the olfactory glomeruli. We measured A β proteins and microglial morphological change. To predict the functional consequences of this pathogenesis in the OB, we examined the dopaminergic neurotransmitter system, a key factor in OSN signalling for the detection of olfactory stimuli [19]. Furthermore, we evaluated ultrastructural changes in the axonal, dendritic, and synaptic structures.

2 | MATERIALS AND METHODS

2.1 | Tissue collection

Post-mortem fresh frozen OBs were obtained from the Netherlands Brain Bank (NBB) (www.brainbank.nl) in Amsterdam, The Netherlands. The NBB received permission to perform autopsies and use tissue and medical records from the Ethical Committee of the Vrij Universiteit (VU) Medical Center (Registration number NHB Project 1147). All donors provided informed consent for autopsies and the use of their brain tissue for research purposes. The post-mortem tissues were stored as non-paraformaldehyde (PFA) fixed fresh frozen tissue.

2.2 | Specimens

A total of 13 subjects were selected based on the Braak stages [20] and ApoE/A β levels, including seven healthy CTLs and six AD patients (Table 1). All AD patients were classified into *Braak* stage 6, of which half harboured two ϵ 4 alleles of *apoE*. One subject was excluded from subregional analysis because of distorted OB tissue. Therefore, the n-number in the AD group is 5 for some parts of our analysis. Age and sex were not statistically different between the two groups (healthy CTLs: four women + three men; AD patients: four women + two men; mean \pm SD of age: healthy CTLs vs AD patients: 77 ± 12.1 vs 76 ± 7.3 years; $p = 0.91$). For unbiased protein immunostaining results, the post-mortem delay (PMD) time was also similar in the two groups (healthy CTLs: 7.3 ± 2.1 [h]; AD: 5.4 ± 0.9 ; $p = 0.1$) (Table 2).

The specimens were stored at -80°C upon arrival at Maastricht University. Tissues for immunohistochemistry were embedded in cryo-embedding medium, optimal cutting temperature (OCT) compound and were cut into $40\ \mu\text{m}$ sections in 10 series and mounted on Superfrost® Plus slides (VWR, Leuven, Belgium) at a working temperature of -20°C . Given the anterior-posterior orientation of the OBs, coronal sections were prepared for optimal stereological analysis (Figure S1). Each series

was processed immunohistochemically and subjected to stereological quantification.

2.3 | Immunohistochemistry

Slides were air-dried for 30 min at 37°C and post-fixed with 4% PFA buffer for 20 min at 4°C . After washing in Tris-buffered saline (TBS) (pH=7.5) for 10 min three times, slides were incubated with TBS-Triton (TBS-T) (0.3%) containing 3% normal donkey serum (NDS) for 30 min. Each series of sections was incubated with one of the following primary antibodies (diluted 1:100–500 in accordance with the manufacturer's instruction in TBS-T with 3% NDS): mouse anti-6E10, a marker for A β (Covance); rabbit anti-A11, a marker for oligomeric A β (Thermo); mouse anti-VGLUT2 (Novus Biologicals); rabbit anti-tyrosine hydroxylase (TH) (Santa Cruz); chicken anti-MAP2 (Abcam); and rabbit anti-IBA1 (Wako) for 48 h at 4°C in a humidified chamber. On the third day, the sections were washed with TBS-T, TBS, and TBS-T (in this order) for 10 min each and then incubated with secondary antibodies (Invitrogen; diluted 1:200–500 in TBS-T with 3% NDS), including donkey anti-rabbit Alexa Fluor 488 (against A11, IBA1), Alexa Fluor 647 (against TH), anti-mouse Alexa Fluor 488

TABLE 1 Subject information

Description	Case #	Sex	Age	PMD	Braak	Amyloid level	APOE	Note
<i>CTL</i>								
CTL 1	S01/016	F	64	8.5	0	B	42	CTL
CTL 2	S12/002	M	55	7	0	B	43	CTL
CTL 3	S11/111	M	93	5	1	O	33	CTL
CTL 4	S03/035	F	82	11.5	1	O	33	CTL
CTL 5	S09/134	F	84	7	1	O	33	CTL with infarction
CTL 6	S14/029	F	78	7	1	A	33	CTL
CTL 7	S13/016	M	83	5	1	A	33	CTL
<i>AD</i>								
AD 1	S15/013	F	73	7.5	6	C	33	AD with CAA and neurofibrillary tangles
AD 2	S12/125	M	71	6.5	6	C	33	AD
AD 3	S14/049	F	78	5	6	C	44	AD with CAA and cotton wool plaques
AD 4	S13/040	F	70	4.5	6	C	44	AD
AD 5	S15/040	M	76	5	6	C	44	AD with CAA, amygdala α -synucleinopathy and hippocampal sclerosis
AD 6	S13/036	F	90	4	6	C	32	AD with, small infarction in CA1 and in putamen left

Abbreviations: AD, Alzheimer's disease; CA, cornu ammonis; CAA, cerebral amyloid angiopathy; CTL, non-demented control; PMD, post mortem delay (h).

TABLE 2 Demographics and descriptive statistics of subjects

Parameters	CTL		AD		<i>p</i> -value
	Mean	SD (\pm)	Mean	SD (\pm)	
Subject	7		6		–
Sex	Female: 4 Male: 3		Female: 4 Male: 2		>0.05 ^a
Age (years)	77	12.1	76	7.3	0.91 ^b
PMD (h)	7.3	2.1	5.4	0.9	0.10 ^b

Abbreviations: AD, Alzheimer's disease; CTL, non-demented control; PMD, post mortem delay (h); SD, standard deviation.

^aSex was compared using two-way ANOVA.

^bAge and PMD were compared using two-tailed unpaired Welch's *t*-test.

(against 6E10, VGLUT2), and anti-chicken Alexa Fluor 647 (against MAP2), for 2 h at room temperature (RT) in a humidified chamber. After washing in TBS for 10 min three times, the sections were incubated with Hoechst 33342 (diluted 1:10,000) for 10 min at RT. After washing in TBS for 10 min three times, slides were submerged for 10 min in 0.3% Sudan black solution to avoid auto-fluorescence. After washing rapidly eight times in TBS, slides were mounted using 80% glycerol in PBS.

2.4 | Fluorescence density measurement

The expression of 6E10 and A11 was measured using fluorescence density measurement. Images were taken with a stereology microscope connected to an Olympus BX51WI using 10 \times or 20 \times objectives. ImageJ (ver. 1.51j8, NIH, USA) was used for fluorescence intensity measurement, which was quantified using the region of interest (ROI) using the function 'Measure' in ImageJ. For data-colour coherence, the fluorescence of VGLUT2 and MAP2 of adjusted to pseudo-colour using a function of 'Look Up Table' in ImageJ (Figure 1G,H). The threshold was calculated based on negative control sections both in the CTL and AD sections.

2.5 | Cell counting and area/volume measurement

Images were taken with a stereology microscope coupled to an Olympus BX51WI using 10 \times or 20 \times objectives. Stereo Investigator (ver. 11, MBF Bioscience, USA) and ImageJ (ver. 1.51j8, NIH, USA) software were used for cell counting and calculating the cross-sectional area, as previously reported [21]. TH-positive periglomerular cells co-labelled with Hoechst-nuclei were counted using 'Optical Fractionator' in Stereo Investigator. For unbiased quantification, the number and area of individual glomeruli were measured from the same 'ROI' using the function 'Measure' in ImageJ. We used the images taken after Hoechst counterstaining. The volume of every part

was calculated by multiplying the surface with the section thickness and the number of slices per series. Finally, all these parts were summed, and the total volume of the OBs was calculated.

2.6 | Evaluation of microglial morphology

We assessed the microglial reactivation in the glomeruli by quantifying the number and morphology of IBA-1-positive microglial cells. Images were taken with a stereology microscope connected to an Olympus BX51WI using a 20 \times objective and analysed with ImageJ software. The number, size, and morphology of IBA-1 positive microglial cells were quantified based on previously published criteria [22, 23]. Based on their morphology, IBA-1-positive microglial cells were divided into four types, including ramified, hyper-ramified, bushy, and amoeboid, and were further subjected to quantification (Figure 4J–M). For unbiased quantification, the IBA-1 positive microglial cells were assessed in the same 'ROI' using the 'Measure' function in ImageJ.

2.7 | Three-dimensional reconstruction of the olfactory bulb

Three-dimensional reconstruction from serial sections of the OB was conducted to assess the structure, volume, and distribution of different markers across the OB (Video S1). For this reconstruction, the images were taken using stereology microscopes connected to an Olympus BX51WI camera. We used images taken after immunostaining for VGLUT2 and MAP2 and Hoechst counterstaining. The images were stacked using the 'Stitching' tool in ImageJ (ver. 1.51j8). Immunofluorescence images were fed into a virtual structure using a Stereo Investigator software. Contoured Images were aligned according to the reference point and fiducial point. Reconstruction was completed using the 'Reconstruction' function (https://www.mbfbioscience.com/help/si11/Content/SSR/SSR_image_Multi1.htm) [24].

2.8 | Electron microscopy

Tissue preparation and fixation were performed based on a published protocol [25]. In brief, the ventral part of the freshly frozen OB was carefully punched to extract approximately 1 mm³ of a glomerular layer. Then, tissue was immediately immersed in freshly prepared ice-cold 1.5% PFA in PBS, followed by overnight incubation in the same solution at 4°C. Thereafter, the tissue was post-fixed in 3% glutaraldehyde, post-fixed in osmium tetroxide, dehydrated in ethanol, and embedded in Epon (EMS, Hatfield, USA). Sections were cut into 70-nm ultra-thin sections. Ultra-thin

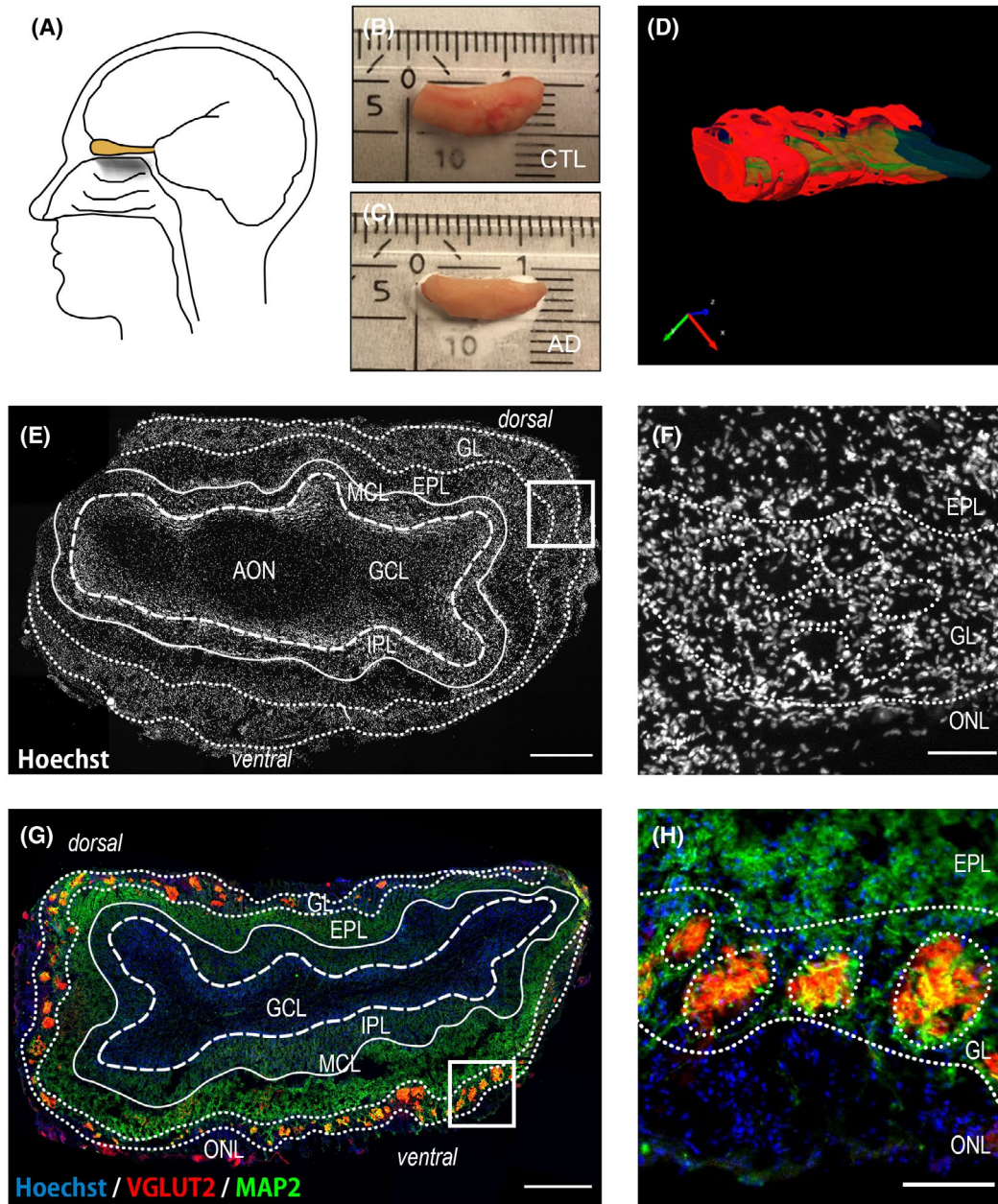


FIGURE 1 Gross morphology of the human olfactory bulb (OB). Schematic representation of the human OB (A) OB specimens obtained from an 80-year-old healthy control, and a 73-year-old Alzheimer's disease patient (B and C respectively). Screenshot represents the three-dimensional reconstruction of the human OB (blue: outer boundaries of the OB; red: glomerular layer; green: granule cell layer (D). A coronal OB section, stained with Hoechst, showing the laminar organisation of the OB (E; scale bar = 500 μ m). The olfactory glomeruli are shown in a coronal OB section (F; scale bar 100 μ m). A coronal OB section was immunohistochemically stained for MAP2 (green) and VGLUT2 (red) and counterstained with Hoechst stain (blue) showing the distribution of the glomeruli across the OB (G; scale bar = 500 μ m). The neuropil structure of the olfactory glomeruli is shown in a coronal OB section (H; scale bar = 100 μ m). A, anterior; AD, Alzheimer's disease; CTL, age-matched control; D, dorsal; L, lateral; M, medial; MAP2, microtubule-associated protein 2; OB, olfactory bulb; P, posterior; V, ventral; VGLUT2, vesicular glutamatergic protein 2

sections were prepared for transmission electron microscopy according to a routine procedure for sample processing. Transmission electron microscopy was conducted using a Tecnai G2 Spirit BioTWIN electron microscope (Thermo Fisher Scientific, Eindhoven, The Netherlands) coupled with an Eagle 4kx4k digital camera (Thermo Fisher Scientific, Eindhoven, The Netherlands). Several tissue overview images were

captured and evaluated for possible damage induced by the freezing procedure. From the overview, higher magnification images were selected in areas not presenting any visible freezing damage, and areas within the captured images of the electron micrographs were observed. When interpreting images, we took into account the criteria that had been described in an earlier study on AD brains [26].

2.9 | Subregional analysis of the olfactory bulb

The OB was assessed based on arbitrarily defined dorsal and ventral subregions (Figure S2). In the frontal anatomical plane, the part of the OB that faced the ventral surface of the frontal lobe was defined as the dorsal half, and the opposite half was named the ventral OB (Figure 1A–D).

Principal component analysis (PCA) was used for multivariate analysis of distinct pathological factors to construct a predictive model for neurodegeneration in the above-mentioned subregions of the OB. Eleven parameters were used for PCA analysis, including age; Braak stage; *apoE4*; the number and size of glomeruli; expression of A β and TH; and the number of ramified, hyper-ramified, bushy, and amoeboid microglia in 13 subjects in each dorsal/ventral region of the olfactory glomeruli. PCA was conducted using the ‘prcomp ()’ function in R (ver. 3.6.3). PCA plots were clustered using the ‘ggplot ()’ and ‘fviz_pca_ind ()’ functions in R.

2.10 | Statistical analysis

General statistics were calculated using GraphPad Prism software (ver. 7.0). Values are presented either as the mean and standard error of the mean or as the mean and coefficient of error. Normal distribution of the data was proved using two-tailed unpaired Welch's *t*-test and two-way ANOVA together with Sidak's post hoc test. Data were checked for outliers using the ROUT method ($Q = 1\%$). Age and sex were used as confounding factors in the analyses. During experiments, the experimenter was blinded to the experimental condition to prevent biased assessment.

3 | RESULTS

3.1 | Gross morphology analysis of the olfactory glomerulus

In Nissl/Hoechst staining, the CTL OB exhibited a laminar organization (Figure 1E). The olfactory glomerular layer had discrete spherical assemblies located at the outer layer of the OB (Figure 1F). Detailed inspection of the section stained with antibodies against MAP2 and VGLUT2 revealed the neuropil structure of the olfactory glomeruli containing presynaptic vesicles markers and dendritic fibres in the outer layer of the OB (Figure 1G, H).

We then quantified the number and size of the glomeruli in the AD samples and CTLs samples (Figure 2). Quantitative volumetry revealed a significant reduction in the volume of the glomerular layer in AD samples compared to that in CTL samples (CTL = 1.00,

AD = 0.73, $p = 0.0477$) (Figure 2A). However, the total number of glomeruli did not differ between the AD and CTL samples (CTL = 1.00, AD = 1.04, $p = 0.8005$) (Figure 2B). In contrast, the quantitative analysis revealed a significant reduction in average glomerular cross-sectional area in the AD samples compared to that in CTL samples (CTL = 1.00, AD = 0.58, $p = 0.0011$) (Figure 2C). Similar changes were observed in the dorsal and ventral subregions of the OB; the total number of glomeruli (CTL-D = 1.00, AD -D = 1.58, CTL-V = 2.11, AD-V = 2.09, $p > 0.05$) (Figure 2D); and the average glomerular cross-sectional area (CTL-D = 1.00, AD-D = 0.58, CTL-V = 1.06, AD-V = 0.65, $p < 0.05$) (Figure 2E).

3.2 | β -Amyloid immunohistochemistry

Qualitative inspection revealed a robust expression of A β in the glomerular layer and to a lesser extent in areas adjacent to the mitral cell layer (Figure 3; CTL: a, c and e; AD: b, d and f). A β was mostly expressed inside the olfactory glomeruli (Figure 3B). In addition, the 6E10 was co-localised with A11 immunoreactivity (Figure S3A). Quantitative analysis showed that A11 immunoreactivity was also higher in the glomeruli of AD patients than in the glomeruli of CTLs (Figure S3B).

Quantitative analysis showed a significant difference in A β expression (6E10- immunoreactivity) in olfactory glomeruli in AD samples compared to that in CTL samples (CTL = 1.00, AD = 3.09 arbitrary unit [au], $p = 0.0062$) (Figure 3G).

The distribution of A β protein was significantly higher in the ventral than in dorsal glomeruli (CTL-D = 1.00, AD-D = 4.62, $p > 0.05$, CTL-V = 1.48, AD-V = 11.74, $p < 0.01$) (Figure 3H). The ratio of A β protein expression in the ventral glomeruli varied across AD patients, ranging from a fold increase of 1.24 (AD 2) to that of 28.14 (AD 6) (Figure 3I,J).

3.3 | Microglia immunohistochemistry

We compared the presence of microglia in the glomerulus between CTL (Figure 4A,C) and AD (Figure 4B,D) subjects and observed that there was more robust infiltration of reactive microglia in the olfactory glomeruli of AD patients (Figure 4B,D).

The number of the IBA-1-positive microglial cells was increased in the ventral glomeruli and increased to a lesser extent in the dorsal glomeruli. Quantitative analysis revealed a more than two-fold increase in the number of IBA-1-positive microglial cells in the glomeruli of AD patients than in the glomeruli of CTLs (CTL = 1.00, AD = 2.35, $p = 0.0048$) (Figure 4E). Both dorsal and ventral glomeruli showed increased immunoreactivity, although the number of IBA-1 positive cells

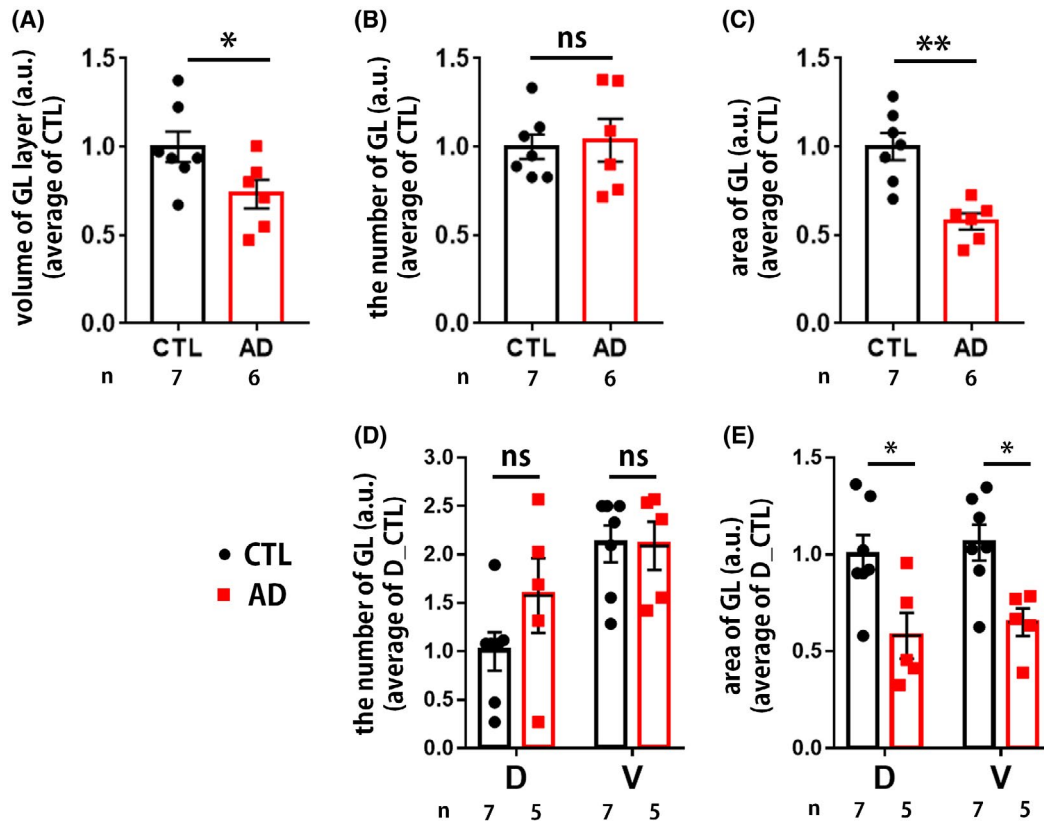


FIGURE 2 Quantification of structural alterations in the olfactory bulb. Graphs show the quantification of the structural alterations in the olfactory glomeruli of healthy controls and Alzheimer's disease patients (A–C). The volume of the glomerular layer (A). The number of glomeruli (B). The cross-sectional area of glomeruli (C). The number of glomeruli in the dorsal and ventral OB subregions (D). The cross-sectional area of the glomeruli in the dorsal and ventral OB subregions (E). In (A–C), two-tailed unpaired Welch's *t*-test was performed; in (D, E), two-way ANOVA together with Sidak's post hoc test was performed. Statistical significance: non-significant, (ns); * $p < 0.05$; ** $p < 0.01$. AD, Alzheimer's disease; au, arbitrary unit; CTL, age-matched control; D, dorsal; GL, glomerulus; n, the number of subjects; V, ventral

was higher in ventral olfactory glomeruli (CTL-D = 1.00, AD-D = 2.21, $p < 0.01$, CTL-V = 1.40, AD-V = 3.44, $p < 0.001$) (Figure 4F). The size of the IBA-1-positive microglial cell bodies was significantly larger in AD patients than in CTLs (CTL = 1.00, AD = 1.76, $p = 0.0011$) (Figure 4G). The cell size values were greater in the ventral OB glomeruli than in the dorsal OB glomeruli (CTL-D = 1.00, AD-D = 1.38, $p > 0.05$, CTL-V = 0.90, AD-V = 1.96, $p < 0.001$) (Figure 4H).

Moreover, the microglial cell body size was increased, and their morphology shifted toward reactive states in the olfactory glomeruli of AD patients. Quantification of microglial morphology demonstrated that the microglia in the normal glomeruli were in ramified, hyper-ramified, bushy, or amoeboid form with the following ratio: 0.38:0.21:0.37:0.04 (Figure 4I). In AD-glomeruli, this ratio was 0.17:0.13:0.33:0.36 (Figure 4I). There was a sharp decline in the number of ramified forms (CTL = 1.00, AD = 0.45, $p < 0.001$) (Figure 4R) and a rise in the number of amoeboid forms (CTL = 1.00, AD = 0.45, $p < 0.001$) (Figure 4U) but not in the number of hyper-ramified and bush forms in AD samples compared to that in CTL samples (Figure 4S,T). The

number of ramified microglia decreased significantly in the ventral part (CTL-D = 1.00, AD-D = 0.61, $p > 0.05$, CTL-V = 0.88, AD-V = 0.33, $p < 0.05$) (Figure 4V). The number of hyper-ramified and bushy form microglia was not different in dorsal vs ventral part in CTL and AD (CTL-D = 1.00, AD-D = 0.93, $p > 0.05$, CTL-V = 1.18, AD-V = 0.54, $p > 0.05$) (Figure 4W), (CTL-D = 1.00, AD-D = 1.01, $p > 0.05$, CTL-V = 1.22, AD-V = 0.97, $p > 0.05$) (Figure 4X). The proportion of the amoeboid form increased in both sides, although the increase in ventral side was more significant (CTL-D = 0.55, AD-D = 3.27, $p < 0.01$, CTL-V = 0.00, AD-V = 6.06, $p < 0.001$) (Figure 4Y).

3.4 | Tyrosine hydroxylase immunohistochemistry

Qualitative inspection revealed that TH-positive periglomerular cells were co-labelled with Hoechst-nuclei, and the fibres were intertwined within the neuropil structure (Figure 5A,C). However, in AD-OB, the TH-positive neurites were rarely visible (Figure 5B,D).

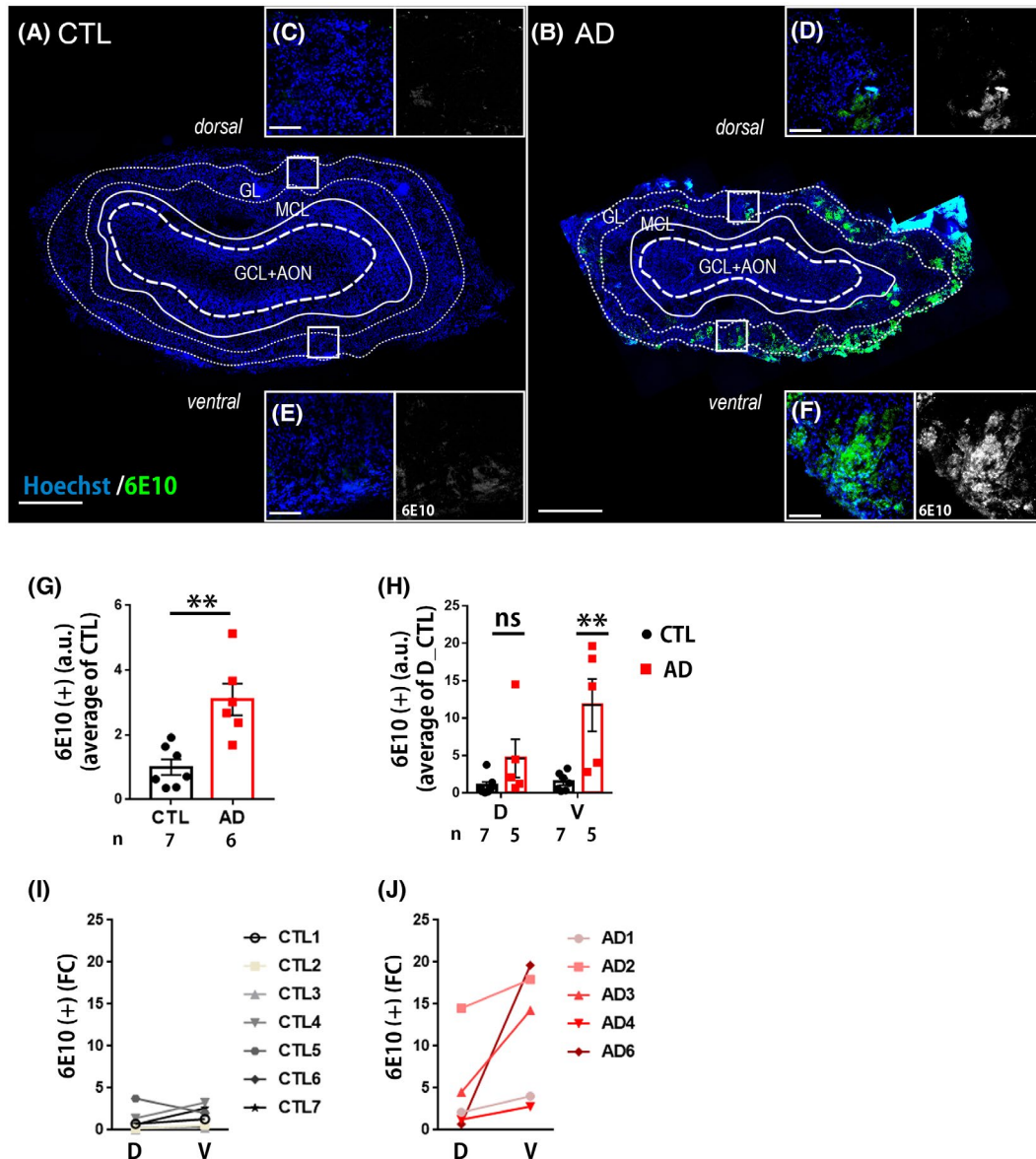
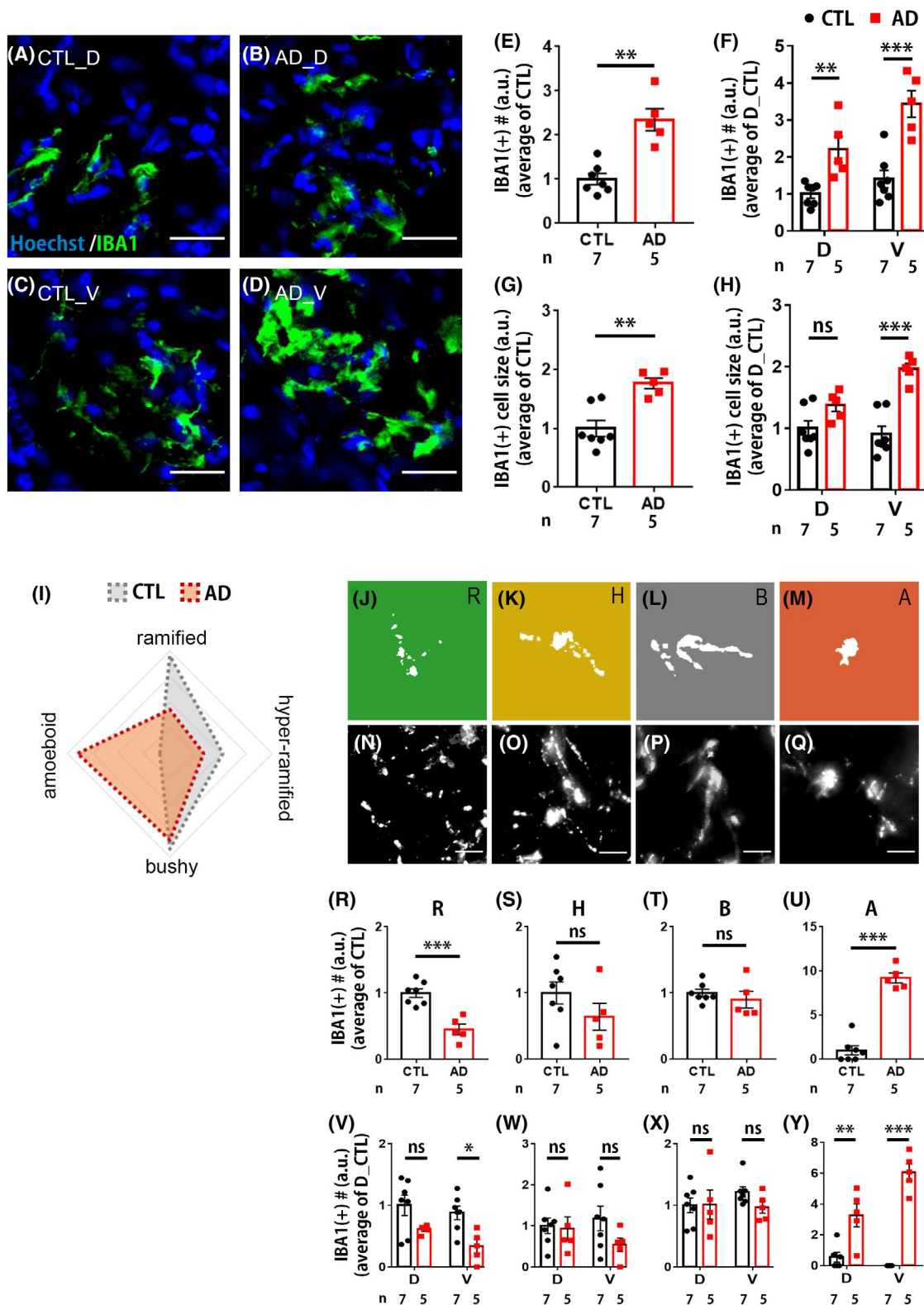


FIGURE 3 Representative images of coronal olfactory bulb sections immunohistochemically stained for 6E10. Images show A β expression in the healthy controls (CTLs) (A) and Alzheimer's disease (AD) patients (B). Magnified 6E10 staining in the dorsal olfactory glomeruli (C, D) and ventral olfactory glomeruli (E, F). Graph shows the quantification of 6E10 expression in the olfactory glomeruli of healthy CTLs and AD patients (G). Quantification of the subregional distribution of 6E10 in the dorsal and ventral olfactory glomeruli (H). Domain distribution of fold changes in CTLs (I) and AD patients (J). In graphs (G) and (H), two-tailed unpaired Welch's *t*-test and two-way ANOVA together with Sidak's post hoc test were performed respectively. Scale bar: 500 μ m (A, B), 250 μ m (C–F). Statistical significances: non-significant (ns); **p* < 0.05; ***p* < 0.01. +, positive signal; AD, Alzheimer's disease; AON, anterior olfactory nucleus; au, arbitrary unit; CTL, age-matched control; D, dorsal; FC, fold change; GCL, granule cell layer; GL, glomerular layer; MCL, mitral cell layer; n, the number of subjects; V, ventral

FIGURE 4 Photomicrographs of olfactory bulb sections immunohistochemically stained for IBA-1. Images show microglia cells in the olfactory bulb (OB) glomeruli of healthy controls (CTLs) and Alzheimer's disease (AD) patients (A–D). Graphs show quantitative data pertaining to the number (E), dorsal vs ventral distribution (F), and size (G) of the IBA-1 positive microglial cells in the OB of CTLs vs AD patients. The size of the IBA-1-positive microglial cells in the dorsal vs ventral OB (H). Distribution of microglial with different morphology in olfactory glomeruli of CTLs and AD patients (I). Different types of microglial morphology in the human olfactory glomerulus (J–Q). Quantitative data pertaining to the number of microglia with ramified (R), hyper-ramified microglia (S) bushy (T), and amoeboid (U) morphology in the OB of CTLs vs AD patients. Graphs “V–Y” show quantitative distributing of the ramified (V), hyper-ramified (W), bushy (X), and amoeboid (Y) microglia in the dorsal vs ventral glomeruli in the OB of CTLs and AD patients. Scale bar 25 μ m (A–D), 10 μ m (N–Q). In (E), (G), and (R–U), two-tailed unpaired Welch's *t*-test was performed; and in (F), (H), and (V–Y), two-way ANOVA together with Sidak's post hoc test was performed. Statistical significances: non-significant (ns); **p* < 0.05; ***p* < 0.01; ****p* < 0.001. A, amoeboid; AD, Alzheimer's disease; B, bushy; CTL, age-matched control; D, dorsal; H, hyper-ramified; n, the number of subjects; R, ramified; V, ventral



We quantified the number of TH-positive periglomerular cells, which were co-labelled with Hoechst. The quantitative cell count showed that AD-glomeruli had fewer TH-periglomerular cells than CTL-glomeruli (CTL = 1.00, AD = 0.43, $p = 0.0011$) (Figure 5E). The

lack of TH-positive periglomerular cells was more prominent in the ventral side of the olfactory glomeruli than in the dorsal side in AD patients (CTL-D = 1.00, AD-D = 0.63, $p > 0.05$, CTL-V = 1.43, AD-V = 0.42, $p < 0.001$) (Figure 5F).

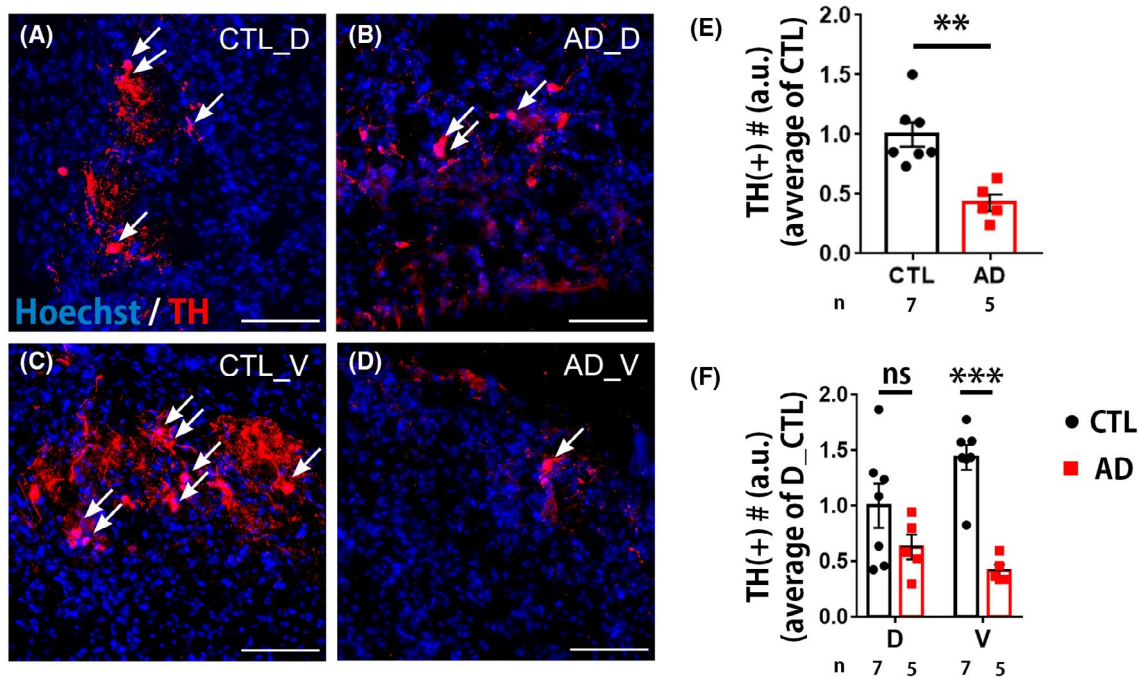


FIGURE 5 Photomicrographs of olfactory bulb sections immunohistochemically stained for tyrosine hydroxylase. Photomicrographs taken from the olfactory bulb (OB) sections immunohistochemically stained for tyrosine hydroxylase (TH). Images show the TH-positive cells in the OB glomeruli of CTLs and AD patients (A–D). The graph shows the quantification of TH expression in the olfactory glomeruli of CTLs and AD patients (E). Quantitative data pertaining to the number and dorsal/ventral distribution of TH-positive periglomerular cells in the OB of CTLs and AD patients (F). Scale bar 100 μ m. In graphs “E, F” two-tailed unpaired Welch’s *t*-test and two-way ANOVA together with Sidak’s post hoc test were performed respectively. Statistical significances: non-significant (ns); ** $p < 0.01$; *** $p < 0.001$. AD, Alzheimer’s disease; CTL, age-matched control; D, dorsal; n, the number of subjects; V, ventral

3.5 | Subregional clustering of the variables

We reassessed the investigated variables based on the regional distribution of changes in the OB region. Using PCA, ‘dimensionality reduction’ data processing was conducted on input variables to create a predictive model based on the anatomical and pathological changes observed in this study. PCA analysis indicated an overlapping pattern of the alterations between CTL and AD samples in the dorsal OB region (Figure 6A), whereas it showed distinctively clustered alterations between CTL and AD in the ventral OB region (Figure 6B).

3.6 | Ultrastructure analysis of the olfactory glomerulus

The ventral glomerular layer of the OB was assessed for ultrastructural changes using electron microscopy. Detailed inspection of the images obtained from AD specimens revealed neuropil threads containing constricted filaments (Figure 7A–C). However, in the dendrites, those constricted filaments were present to a lesser extent (Figure 7A,B). These highly constricted filaments had the appearance of dense inclusions (Figure 7C). In CTL specimens, the synapses contained dense postsynaptic areas and abundant synaptic vesicles (Figure 7D,E). In contrast, the synaptic clefts

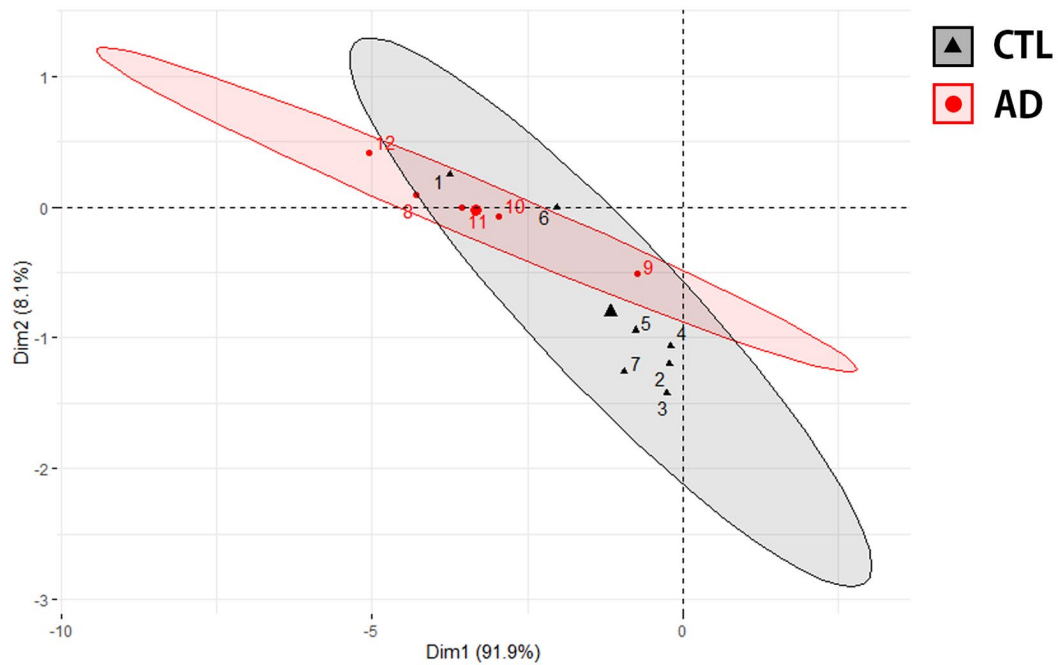
in AD were lost, the synaptic structure was distorted, and greater distances between synapses were observed (Figure 7F,G).

4 | DISCUSSION

Herein, we assessed the morphological and histological alterations in the OB obtained from patients with advanced AD and compared them with those in matched CTLs (Figure 8). We found robust expression of the pathological hallmarks of AD, such as $A\beta$ accumulation, in the OB of AD patients, especially in the olfactory glomerular layer, where the first synapse is formed with the OSN. $A\beta$ accumulation co-existed with additional histological alterations such as infiltration of reactivated microglia and severe atrophy, mainly caused by loss of periglomerular cells. Advanced PCA indicated a predominantly ventral deficit in the glomeruli (Figure 6, Table 3).

The OB constitutes a layered structure with specific cell types and functions in each layer. The functional characteristics and structural integrity of each layer and the OB are critical for its activity [27]. Our results showed a severe shrinkage of the olfactory glomerular layer that could affect signal transduction between OE and OB neurons and could lead to significant disruption in olfactory detection (Figure 2). Electron microscopy

(A) dorsal



(B) ventral

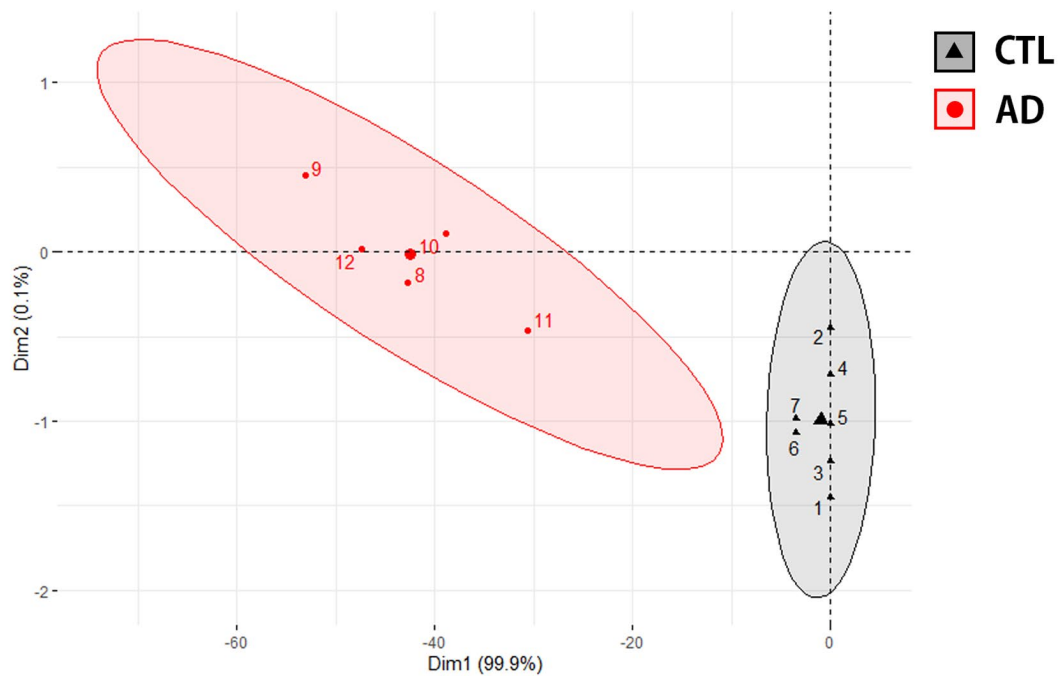


FIGURE 6 Principal component analysis plot of distinct pathological factors in the dorsal and ventral glomeruli of the olfactory bulb. Principal component analysis (PCA) plot of distinct pathological factors in the dorsal (A) and ventral (B) glomeruli of the olfactory bulb (OB) in healthy controls and Alzheimer's disease patients. Unit variance scaling was applied to rows, and singular value decomposition with imputation was used to calculate principal components. X and Y axis show principal component 1 and 2 which explain (a) 91.9%, (b) 8.1% and (a) 99.9%, (b) 0.1% of the total variance respectively. Prediction ellipses exhibit 0.95 probability. $n = 7$ (CTL), 5 (AD) data points. AD, Alzheimer's disease; CTL, age-matched control

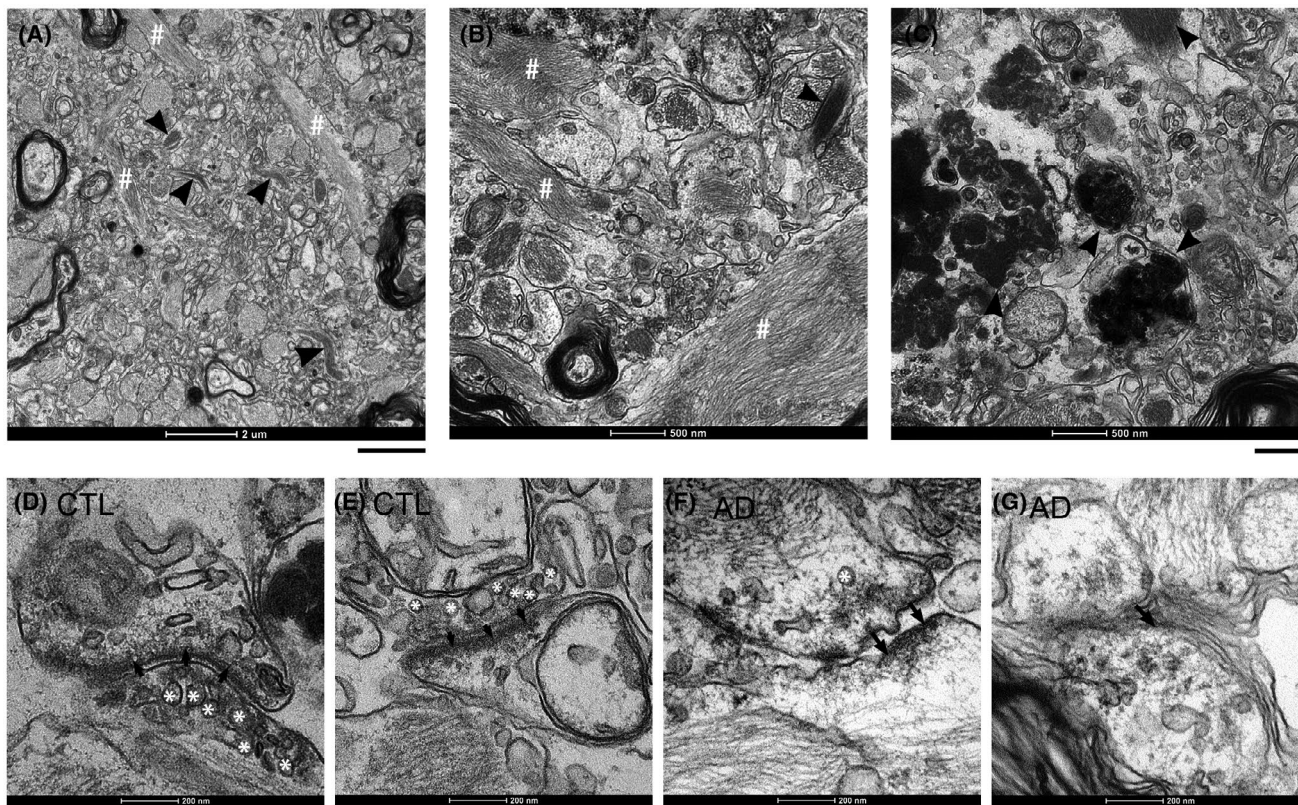


FIGURE 7 The ultrastructure of the olfactory glomerulus. The ultrastructure of the olfactory glomerulus in Alzheimer's disease (AD) (A–C). Arrowheads indicate neuropil threads formed by constricted dendritic filaments (A–C). Sharp lines are slightly constricted filaments in neuropil threads in AD dendrites (A, B). Arrowheads in (C) indicate highly constricted filaments (dense bodies). The ultrastructure of synapse in the olfactory glomerulus in healthy control (D, E) and AD (F, G). White asterisks and black arrows indicate synaptic vesicles and postsynaptic densities respectively (D, E). Scale bar 2 μm (A), 500 nm (B, C), 200 nm (D–G). AD, Alzheimer's disease; CTL, age-matched control

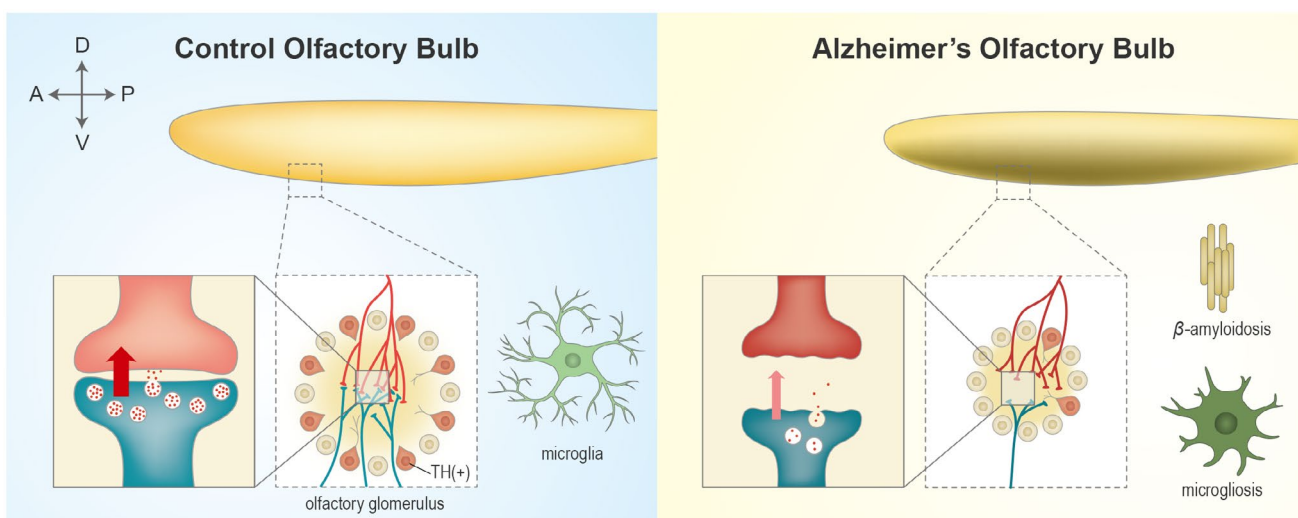


FIGURE 8 Alterations in human olfactory glomeruli with high β -amyloid burden in Alzheimer's disease. A, anterior; AD, Alzheimer's disease; D, dorsal; OB, olfactory bulb; P, posterior; TH, tyrosine hydroxylase; V, ventral

of the glomeruli revealed detectable damage in this area, in accordance with our histological findings (Figure 7). In the electron microscopy images, neuropil threads

containing constricted filaments were observed, which affected dendrites that also shared similar features, as revealed in an earlier study on AD brains [26]. During

TABLE 3 Subregional analysis between AD and CTL

Type	Quantifying factors	Dorsal			Ventral		
		CTL	AD	CTL vs AD ($p^{\#}$)	CTL	AD	CTL vs AD (p)
Anatomy I	glomerular #	1.00	1.58	ns	2.21	2.09	ns
Anatomy II	glomerular area	1.00	0.58	↓ (*)	1.06	0.65	↓ (*)
Pathology I	β-amyloid	1.00	4.62	Ns	1.48	11.74	↑ (**)
Pathology II	reactive microglia	1.00	1.38	ns	0.90	1.96	↑ (***)
Physiology	tyrosine hydroxylase	1.00	0.62	ns	1.43	0.42	↓ (***)

Abbreviations: AD, Alzheimer's disease; CTL, non-demented control.

P -value: A two-way ANOVA together with Sidak's post hoc test was performed. Statistical significances are denoted as follows: non-significant (ns); * p < 0.05; ** p < 0.01; *** p < 0.001.

the qualitative inspection of the synaptic ultrastructure, we observed distorted postsynaptic densities and fewer presynaptic vesicles in AD specimens that could be a contributing factor to synaptic failure in the glomeruli and the eventual olfactory dysfunction, which is known to be a common symptom in AD patients. Impaired synaptic transmission between the OSNs and mitral/tufted cells may explain compromised processing of odour stimuli in general [28]. It could lead to degeneration of periglomerular cells, which disrupts the lateral inhibition processes critical for sharpening sensory inputs and eventually discriminating odorants [19].

Our PCA analysis showed apparent dissimilarities in the distribution of degeneration along the dorsal-ventral axis of the OB (Figure 6). This was in line with the findings from our previous rodent studies suggesting that region-specific degeneration and pathogenesis might be associated with the topographical organization of the OB [29]. In the murine OE, spatial cues within the tissue can direct the spatially restricted differentiation of the OSN, critical for normal olfactory function [30]. OSNs, in turn, play a prominent role in defining the structural organization and cellular composition of the glomeruli [31]. According to our findings, it is plausible that a toxic event caused by spatial A β accumulation and inflammation leads to ventrally oriented dysregulation of the OSNs' axon convergence toward the glomerulus and abnormal effects on the structural integrity of the OB. We propose that the ventrally oriented OB deficit observed in this study was predominantly caused by an impaired interaction between the OSNs and olfactory neurons (mitral and tufted cells) in the glomeruli. Interestingly, the volumetric analysis showed that OB shrinkage was mainly caused by atrophy of the glomeruli rather than a change in their numbers (Figure 2). This provides additional evidence that impaired convergence of OSNs' axons toward the glomerulus could be the cause of tissue loss. Although some deficits were evenly distributed across the dorsal-ventral axis of the OB, such as increased microglia reactivity, these changes could be a consequence of systemic deficits beyond the OSNs' convergence to the OB. Topographic organization of the

olfactory glomerulus has been well characterized in rodents [6, 9]. A recent study points toward the existence of this segregation in the human olfactory glomerulus as well [32]. Moreover, predominantly ventral deficits in the OB have also been reported along the dorsal-ventral axis in patients with advanced Parkinson's disease who also exhibit olfactory dysfunction [32]. These results suggest that regional differences in vulnerability and resilience towards degeneration may exist in the primary olfactory system in AD. In addition, their finding is consistent with the 'olfactory vector hypothesis' for the pathogenesis of this neurodegenerative disease [33]. Based on their hypothesis, the olfactory system may provide a potential route, which can trigger neurodegenerative diseases. Microglia monitor the neural system in the resting state [34]. They can sense an inflammatory response and become reactive following infiltration into the site of injury [34]. Reactive microglia undergo several morphological changes based on their activity level [35]. In AD, excessive A β accumulation promotes microgliosis [36]. Furthermore, gliosis is a driving force for A β pathology by sustaining increased A β levels and accelerating the pathological vicious cycle [16]. Although the causal relationship between microglial activation and A β accumulation in olfactory deficits remains elusive, the olfactory glomeruli of AD patients undergo intense pathological alterations following neuroinflammation, which could likely cause olfactory dysfunction.

We observed significant co-labelling of A β -immunoreactivity with oligomeric A β -immunoreactivity primarily in the glomerular layer (Figure S3). Most deposits of A β aggregates co-existed with oligomeric forms in the glomerulus layer (Figure S3). Typically, soluble A β s are cleaved and oligomerized in presynaptic vesicles and released into the extracellular space [13]. These oligomeric A β s accumulate in the extracellular space and induce toxicity [37]. Since 2010, several studies have reported signs of A β amyloidosis and tau pathology in the olfactory areas, including OE and OB [17, 18]. However, those findings have not identified a mechanism by which those neurodegenerative processes would lead to olfactory dysfunction in AD. It remains to be determined

whether the misfolded A β protein originates from the upstream areas in the brain or from OSNs. Altogether, these data indicate that concomitant inflammatory processes and proteopathy occur in the OB of AD patients, similar to that reported in AD brains [38]. This inflammation could further exacerbate the neurodegeneration in the OB, resulting in olfactory malfunction [39].

Despite the limitations of our post-mortem approach, we addressed the potential effects of A β -associated pathology on signal processes in the glomeruli. In periglomerular cells, synaptic transmission is mainly modulated by dopaminergic periglomerular cells [27]. Periglomerular cells mature and express TH by receiving inputs from OSNs and release GABA for lateral inhibition to sharpen the olfactory signals [40]. Therefore, the dopaminergic periglomerular cells can indirectly indicate the functionality of the OSNs [11, 32, 41]. The fate of dopaminergic periglomerular cells depends on excitatory input from the OSNs [19]. After receiving this input from the OSNs, they mature and release dopamine, which is critical for the lateral inhibition that sharpens the odour signals [27]. Therefore, TH expression indicates increased functional inputs from the OSNs [11, 19]. We observed that TH-immunoreactivity was drastically reduced in the glomeruli of AD patients (Figure 5), suggesting the loss of sensory input from the OSNs. This loss of input could be caused by a disrupted synaptic structure and function in the glomeruli, as shown in the electron microscopy assessment (Figure 7). Notably, most studies to date suggest that olfactory abnormalities in AD are because of impaired central information processing rather than sensory dysfunction, namely 'conductive' dysfunction (reviewed in Rey et al. [33]). Nevertheless, our data suggest that next to the neurodegeneration present in the cortical areas, local pathological alterations in the olfactory glomeruli (i.e. structural disintegration) could lead to an olfactory dysfunction in patients with AD as well. Nonetheless, it remains to be determined whether the pathologies in the olfactory glomerulus precede the cortical deficits or occur simultaneously. Given the fact that olfactory dysfunction occurs prior to the onset of clinical cognitive symptoms, one may suggest that at least distinct neurodegenerative processes may involve cortical and OB degeneration in AD.

This study has several limitations. However, we assessed the well-characterized AD patient's olfactory system. Olfactory deficit is an early feature of AD and therefore studying the OBs in MCI or early disease stages could be more relevant. However, we were not able to obtain those tissues, as olfactory bulb (OB) specimens of subjects with MCI or early AD are scarce, or come with severe comorbidities. Moreover, well-characterized AD specimens must meet strict criteria in terms of anatomical hallmarks of the disease as well as clinical history [42]. Moreover, many MCI or early AD brain specimens are obtained from patients with other severe pathologies,

which could lead to misleading postmortem findings [43]. Nevertheless, our study provides novel insights on olfactory glomerulus pathology as the converging point of peripheral and central nervous systems. This concept has been largely unexplored in olfactory dysfunction research in AD. There is ample evidence on microgliosis occurring in central olfactory glomeruli [44]. However, its association with neuropathology in AD has not been proven. In this study, we observed microglia expression around A β deposits that can provide a rationale to further study their association (Figure S4).

Senile plaques and neurofibrillary tangles are among cardinal hallmarks of AD [45]. Different forms of A β molecules are believed to initiate or trigger the mechanisms responsible for tau pathology. For instance, A β accumulation accelerates tau pathology by triggering a pathological cascade in different mouse models [46, 47]. Both A β and tau pathology have been reported in post-mortem AD olfactory glomerulus [18]. Since neurofibrillary tangles originate from the entorhinal cortex [45], and the olfactory circuit is connected to the entorhinal areas, it is plausible that the OB could contribute to the progression of tau pathology. Therefore, further analysis of tau and neurofibrillary tangles need to be conducted in the OB.

Taken together, we observed A β pathology and concomitant A β -associated pathologic alterations in the olfactory glomerulus in AD patients. The olfactory glomeruli showed plausible degeneration with A β accumulation and microgliosis. These alterations, together with the ultrastructural changes at the level of periglomerular cells that regulate neurotransmission by OSNs, indicate that altered glomerular structural integrity may affect OB function in AD. Remarkably, olfactory glomeruli in AD patients were affected to a greater extent on the ventral side (Figure 6, Table 3), suggesting that impaired neuronal interactions could initiate OB degeneration in AD. Therefore, damage to the human olfactory glomerulus with a high A β burden in AD illustrates the potential phenotypic features that explain the olfactory dysfunction in AD. These findings may convey a better understanding of the loss of olfactory sensation in AD patients which has received limited attention so far, providing a better understanding of the underlying mechanisms of AD.

ACKNOWLEDGEMENTS

The authors are grateful to Mrs Hellen Steinbusch for her support for immunohistochemistry and microscopy and to the members of the Microscopy CORE Lab at the Faculty of Health, Medicine and Life Sciences of Maastricht University for their support with electron microscopy.

CONFLICT OF INTEREST

The authors report no competing interests.

AUTHOR CONTRIBUTIONS

Conceptualization: Gowoon Son, Harry W. M. Steinbusch, Cheil Moon and Ali Jahanshahi; Methodology: Gowoon Son, Carmen López-Iglesias and Ali Jahanshahi; Formal analysis and investigation: Gowoon Son and Carmen López-Iglesias; Writing – original draft preparation: Gowoon Son and Ali Jahanshahi; Writing – review and editing: Gowoon Son, Harry W. M. Steinbusch, Carmen López-Iglesias, Cheil Moon and Ali Jahanshahi; Funding acquisition: Cheil Moon; Resources: Ali Jahanshahi; Supervision: Cheil Moon and Ali Jahanshahi, Harry W. M. Steinbusch.

ETHICAL RESPONSIBILITIES OF AUTHORS

The manuscript should not be submitted to more than one journal for simultaneous consideration.

DATA AVAILABILITY STATEMENT

The data that support the findings of this study are available from the corresponding author upon reasonable request.

ORCID

Ali Jahanshahi  <https://orcid.org/0000-0002-7451-3461>

REFERENCES

- Alzheimer's-Association. 2021 Alzheimer's disease facts and figures. *Alzheimers Dement*. 2021.
- Murphy C. Olfactory and other sensory impairments in Alzheimer disease. *Nat Rev Neurol*. 2019;15(1):11–24.
- Espirito DA, Rashid H, Mast BT, Fitzgerald J, Steinberg J, Lichtenberg PA. Depression, cognitive impairment and function in Alzheimer's disease. *Int J Geriatr Psychiatry*. 2001;16(11):1098–103.
- Duff K, McCaffrey RJ, Solomon GS. The Pocket Smell Test: successfully discriminating probable Alzheimer's dementia from vascular dementia and major depression. *J Neuropsychiatry Clin Neurosci*. 2002;14(2):197–201.
- Wilson RS, Arnold SE, Schneider JA, Tang Y, Bennett DA. The relationship between cerebral Alzheimer's disease pathology and odour identification in old age. *J Neurol Neurosurg Psychiatry*. 2007;78(1):30–5.
- Treloar HB, Feinstein P, Mombaerts P, Greer CA. Specificity of glomerular targeting by olfactory sensory axons. *J Neurosci*. 2002;22(7):2469–77.
- Morrison EE, Costanzo RM. Morphology of the human olfactory epithelium. *J Comp Neurol*. 1990;297(1):1–13.
- Tan J, Savigner A, Ma M, Luo M. Odor information processing by the olfactory bulb analyzed in gene-targeted mice. *Neuron*. 2010;65(6):912–26.
- Vassar R, Chao SK, Sitcheran R, Nunez JM, Vosshall LB, Axel R. Topographic organization of sensory projections to the olfactory bulb. *Cell*. 1994;79(6):981–91.
- Storace DA, Cohen LB. Measuring the olfactory bulb input-output transformation reveals a contribution to the perception of odorant concentration invariance. *Nat Commun*. 2017;8(1):81.
- Cao L, Schrank BR, Rodriguez S, Benz EG, Moulia TW, Rickenbacher GT, et al. Abeta alters the connectivity of olfactory neurons in the absence of amyloid plaques in vivo. *Nat Commun*. 2012;3:1009.
- Palop JJ, Mucke L. Amyloid-beta-induced neuronal dysfunction in Alzheimer's disease: from synapses toward neural networks. *Nat Neurosci*. 2010;13(7):812–8.
- Kamenetz F, Tomita T, Hsieh H, Seabrook G, Borchelt D, Iwatsubo T, et al. APP processing and synaptic function. *Neuron*. 2003;37(6):925–37.
- Hsieh H, Boehm J, Sato C, Iwatsubo T, Tomita T, Sisodia S, et al. AMPAR removal underlies Abeta-induced synaptic depression and dendritic spine loss. *Neuron*. 2006;52(5):831–43.
- Sarlus H, Heneka MT. Microglia in Alzheimer's disease. *J Clin Invest*. 2017;127(9):3240–9.
- Wyss-Coray T, Mucke L. Inflammation in neurodegenerative disease—a double-edged sword. *Neuron*. 2002;35(3):419–32.
- Arnold SE, Lee EB, Moberg PJ, Stutzbach L, Kazi H, Han LY, et al. Olfactory epithelium amyloid-beta and paired helical filament-tau pathology in Alzheimer disease. *Ann Neurol*. 2010;67(4):462–9.
- Bathini P, Mottas A, Jaquet M, Brai E, Alberi L. Progressive signaling changes in the olfactory nerve of patients with Alzheimer's disease. *Neurobiol Aging*. 2019;76:80–95.
- Baker H, Kawano T, Margolis FL, Joh TH. Transneuronal regulation of tyrosine hydroxylase expression in olfactory bulb of mouse and rat. *J Neurosci*. 1983;3(1):69–78.
- Thal DR, Rub U, Orantes M, Braak H. Phases of A beta-deposition in the human brain and its relevance for the development of AD. *Neurology*. 2002;58(12):1791–800.
- Golub VM, Brewer J, Wu X, Kuruba R, Short J, Manchi M, et al. Neurostereology protocol for unbiased quantification of neuronal injury and neurodegeneration. *Front Aging Neurosci*. 2015;7:196.
- Crews FT, Lawrimore CJ, Walter TJ, Coleman LG Jr. The role of neuroimmune signaling in alcoholism. *Neuropharmacology*. 2017;122:56–73.
- Zhao X, Liao Y, Morgan S, Mathur R, Feustel P, Mazurkiewicz J, et al. Noninflammatory changes of microglia are sufficient to cause epilepsy. *Cell Rep*. 2018;22(8):2080–93.
- Shi W, Xianyu A, Han Z, Tang X, Li Z, Zhong H, et al. Ontogenetic establishment of order-specific nuclear organization in the mammalian thalamus. *Nat Neurosci*. 2017;20(4):516–28.
- Fortunato F, Hackert T, Buchler MW, Kroemer G. Retrospective electron microscopy: preservation of fine structure by freezing and aldehyde fixation. *Mol Cell Oncol*. 2016;3(6):e1251382.
- Yamaguchi H, Nakazato Y, Shoji M, Ihara Y, Hirai S. Ultrastructure of the neuropil threads in the Alzheimer brain: their dendritic origin and accumulation in the senile plaques. *Acta Neuropathol*. 1990;80(4):368–74.
- Nagayama S, Homma R, Imamura F. Neuronal organization of olfactory bulb circuits. *Front Neural Circuits*. 2014;8:98.
- Wachowiak M, McGann JP, Heyward PM, Shao Z, Puche AC, Shipley MT. Inhibition [corrected] of olfactory receptor neuron input to olfactory bulb glomeruli mediated by suppression of presynaptic calcium influx. *J Neurophysiol*. 2005;94(4):2700–12.
- Son G, Yoo SJ, Kang S, Rasheed A, Jung DH, Park H, et al. Region-specific amyloid-beta accumulation in the olfactory system influences olfactory sensory neuronal dysfunction in 5x*FAD* mice. *Alzheimers Res Ther*. 2021;13(1):4.
- Coleman JH, Lin B, Louie JD, Peterson J, Lane RP, Schwob JE. Spatial determination of neuronal diversification in the olfactory epithelium. *J Neurosci*. 2019;39(5):814–32.
- Morrison FG, Dias BG, Ressler KJ. Extinction reverses olfactory fear-conditioned increases in neuron number and glomerular size. *Proc Natl Acad Sci U S A*. 2015;112(41):12846–51.
- Zapiec B, Dieriks BV, Tan S, Faull RLM, Mombaerts P, Curtis MA. A ventral glomerular deficit in Parkinson's

- disease revealed by whole olfactory bulb reconstruction. *Brain*. 2017;140(10):2722–36.
33. Rey NL, Wesson DW, Brundin P. The olfactory bulb as the entry site for prion-like propagation in neurodegenerative diseases. *Neurobiol Dis*. 2018;109(Pt B):226–48.
 34. Nimmerjahn A, Kirchhoff F, Helmchen F. Resting microglial cells are highly dynamic surveillants of brain parenchyma in vivo. *Science*. 2005;308(5726):1314–8.
 35. Young K, Morrison H. Quantifying microglia morphology from photomicrographs of immunohistochemistry prepared tissue using ImageJ. *J Vis Exp*. 2018;(136):57648.
 36. Frackowiak J, Wisniewski HM, Wegiel J, Merz GS, Iqbal K, Wang KC. Ultrastructure of the microglia that phagocytose amyloid and the microglia that produce beta-amyloid fibrils. *Acta Neuropathol*. 1992;84(3):225–33.
 37. Benilova I, Karran E, De Strooper B. The toxic Aβ oligomer and Alzheimer's disease: an emperor in need of clothes. *Nat Neurosci*. 2012;15(3):349–57.
 38. Ubeda-Banon I, Saiz-Sanchez D, Flores-Cuadrado A, Rioja-Corroto E, Gonzalez-Rodriguez M, Villar-Conde S, et al. The human olfactory system in two proteinopathies: Alzheimer's and Parkinson's diseases. *Transl Neurodegener*. 2020;9(1):22.
 39. Bartels T, De Schepper S, Hong S. Microglia modulate neurodegeneration in Alzheimer's and Parkinson's diseases. *Science*. 2020;370(6512):66–9.
 40. Bonzano S, Bovetti S, Gendusa C, Peretto P, De Marchis S. Adult born olfactory bulb dopaminergic interneurons: molecular determinants and experience-dependent plasticity. *Front Neurosci*. 2016;10:189.
 41. Baker H. Unilateral, neonatal olfactory deprivation alters tyrosine hydroxylase expression but not aromatic amino acid decarboxylase or GABA immunoreactivity. *Neuroscience*. 1990;36(3):761–71.
 42. Carlos AF, Poloni TE, Medici V, Chikhladze M, Guaita A, Ceroni M. From brain collections to modern brain banks: a historical perspective. *Alzheimers Dement (N Y)*. 2019;5:52–60.
 43. Schneider JA, Arvanitakis Z, Leurgans SE, Bennett DA. The neuropathology of probable Alzheimer disease and mild cognitive impairment. *Ann Neurol*. 2009;66(2):200–8.
 44. Kohl Z, Schlachetzki JC, Feldewerth J, Hornauer P, Munch M, Adame A, et al. Distinct pattern of microgliosis in the olfactory bulb of neurodegenerative proteinopathies. *Neural Plast*. 2017;2017:3851262.
 45. Braak H, Braak E. Neuropathological staging of Alzheimer-related changes. *Acta Neuropathol*. 1991;82(4):239–59.
 46. Hurtado DE, Molina-Porcel L, Iba M, Aboagye AK, Paul SM, Trojanowski JQ, et al. Aβ accelerates the spatiotemporal progression of tau pathology and augments tau amyloidosis in an Alzheimer mouse model. *Am J Pathol*. 2010;177(4):1977–88.
 47. Clayton K, Delpech JC, Herron S, Iwahara N, Ericsson M, Saito T, et al. Plaque associated microglia hyper-secrete extracellular vesicles and accelerate tau propagation in a humanized APP mouse model. *Mol Neurodegener*. 2021;16(1):18.

SUPPORTING INFORMATION

Additional supporting information may be found in the online version of the article at the publisher's website.

Supplementary Material

FIGURE S1 Stereological histology experimental scheme. (a) Coronal sectioning of the olfactory bulb. (b) Olfactory bulb sections on glass slide. First of every 10th section was mounted on adhesive glass slides. (c) Section series; each olfactory bulb was cut in five series, each consisting of 10 slides

FIGURE S2 Photomicrographs taken from the sections containing the olfactory bulb (OB) showing the dorsal and ventral subregions; dorsal (D), ventral (V)

FIGURE S3 Distribution of oligomeric Aβ immunohistochemistry in the human olfactory bulb. (A) Immunofluorescence staining for localization of 6E10 and A11, (green) 6E10, (red) A11, (blue) Hoechst. (B) Ratio of A11 immunoreactivity in olfactory glomerulus. Scale bar 100 μm. In (B), two-tailed unpaired *t*-test was performed. Statistical significances are denoted as follows: **p* < 0.05. AD, Alzheimer's disease; CTL, age-matched control

FIGURE S4 Photomicrographs show the olfactory glomeruli immunohistochemically stained for 6E10 and IBA1. Images show the 6E10 and IBA1-positive cells in the OB glomeruli of healthy controls and AD patients (A–D). Three-dimensional illustration of 6E10 and IBA1-positive cells around the olfactory glomeruli (E). Hoechst; blue, 6E10; green, IBA1; red. Scale bar 100 μm. AD, Alzheimer's disease; CTL, age-matched control; D, dorsal; V, ventral

Video S1 Three-dimensional reconstruction of a control olfactory bulb from a normal case based on immunofluorescence of coronal section with antibodies against VGLUT2, MAP2 and Hoechst counterstaining

How to cite this article: Son G, Steinbusch HWM, López-Iglesias C, Moon C, Jahanshahi A. Severe histomorphological alterations in post-mortem olfactory glomeruli in Alzheimer's disease. *Brain Pathol*. 2022;32:e13033. <https://doi.org/10.1111/bpa.13033>